

# On the Orbits and Masses of the Satellites of the Pluto-Charon System

Man Hoi Lee and S. J. Peale

*Department of Physics, University of California, Santa Barbara, CA 93106*

## ABSTRACT

Two small satellites of Pluto, S/2005 P1 (hereafter P1) and S/2005 P2 (hereafter P2), have recently been discovered outside the orbit of Charon, and their orbits are nearly circular and nearly coplanar with that of Charon. Because the mass ratio of Charon-Pluto is  $\sim 0.1$ , the orbits of P2 and P1 are significantly non-Keplerian even if P2 and P1 have negligible masses. We present an analytic theory, with P2 and P1 treated as test particles, which shows that the motion can be represented by the superposition of the circular motion of a guiding center, the forced oscillations due to the non-axisymmetric components of the potential rotating at the mean motion of Pluto-Charon, the epicyclic motion, and the vertical motion. The analytic theory shows that the azimuthal periods of P2 and P1 are shorter than the Keplerian orbital periods, and this deviation from Kepler's third law is already detected in the unperturbed Keplerian fit of Buie and coworkers. In this analytic theory, the periapse and ascending node of each of the small satellites precess at nearly equal rates in opposite directions.

From direct numerical orbit integrations, we show the increasing influence of the proximity of P2 and P1 to the 3:2 mean-motion commensurability on their orbital motion as their masses increase within the ranges allowed by the albedo uncertainties. If the geometric albedos of P2 and P1 are high and of order of that of Charon, the masses of P2 and P1 are sufficiently low that their orbits are well described by the analytic theory. The variation in the orbital radius of P2 due to the forced oscillations is comparable in magnitude to that due to the best-fit Keplerian eccentricity, and there is at present no evidence that P2 has any significant epicyclic eccentricity. However, the orbit of P1 has a significant epicyclic eccentricity, and the prograde precession of its longitude of periapse with a period of 5300 days should be easily detectable. If the albedos of P2 and P1 are as low as that of comets, the large inferred masses induce significant short-term variations in the epicyclic eccentricities and/or periapse longitudes on the 400–500-day timescales due to the proximity to the 3:2 commensurability. In fact, for the maximum inferred masses, P2 and P1 may be in the 3:2 mean-motion resonance, with the resonance variable involving the periapse longitude of P1 librating. Observations that sample the orbits of P2 and P1 well on the 400–500-day timescales should provide strong constraints on the masses of P2 and P1 in the near future.

## 1. INTRODUCTION

Weaver et al. (2006) have recently discovered two new satellites of Pluto, S/2005 P1 (hereafter P1) and S/2005 P2 (hereafter P2), from images taken with the *Hubble Space Telescope* (HST). These are the first new satellites of Pluto since the discovery of Charon in 1978 (Christy and Harrington 1978). The new satellites are much fainter and hence much smaller than Charon (whose diameter  $\sim 1200$  km; e.g., Sicardy et al. 2006), with the diameter of P1  $\sim 60$ – $170$  km depending on the geometric albedo, and P2 about 20% smaller than P1. Since the discovery data consist of only two epochs separated by three days in May 2005, Weaver et al. (2006) were unable to determine the orbits of P2 and P1, but the data are consistent with the orbits of P2 and P1 being nearly circular and nearly coplanar with that of Pluto-Charon, with orbital periods of  $\sim 25$  days for P2 and  $\sim 38$  days for P1. Steffl et al. (2006) have used the same HST observations to place constraints on the existence of any additional satellites of Pluto.

Prior to the discovery of P2 and P1, Buie et al. (2006, hereafter BGYYS) have obtained HST images of the Pluto system in a series of 12 visits from June 2002 to June 2003 for the purpose of producing an albedo map of Pluto. BGYYS were able to detect Charon in individual frames and P2 and P1 by stacking the images taken during each visit. BGYYS fit this data, together with the data for Charon from Tholen and Buie (1997) and the data for P2 and P1 from Weaver et al. (2006), by assuming that all three satellites are on unperturbed Keplerian orbits. The best-fit Keplerian orbital parameters found by BGYYS and their  $1\text{-}\sigma$  errors are reproduced in Table 1. The best-fit orbit of Charon relative to Pluto is consistent with zero eccentricity, and BGYYS pointed out that the nonzero eccentricity reported by Tholen and Buie (1997) is probably due to the use of an imprecise center of body of Pluto in the earlier paper. The parameters in Table 1 show that the orbits of P2 and P1 are indeed nearly circular and nearly coplanar with that of Pluto-Charon. Because P2 and P1 are much smaller than Pluto and Charon, they orbit about a point that is very close to the center of mass of Pluto and Charon. Thus one of the fitting parameters is the mass ratio of Charon-Pluto, and BGYYS found  $m_c/m_p = 0.1165 \pm 0.0055$ .

Two results from the orbit-fitting suggest that unperturbed Keplerian orbits are not good assumptions for the orbits of P2 and P1. The orbital period  $P$  and semimajor axis  $a$  of each orbit are independent parameters in the fits by BGYYS. If we assume that Kepler’s third law is valid for all of the orbits, each orbit yields an independent measurement of the total mass of Pluto-Charon. BGYYS found  $m_p + m_c = 1.4570 \pm 0.0009 \times 10^{22}$  kg from Charon’s orbit,  $1.480 \pm 0.011 \times 10^{22}$  kg from P2’s orbit, and  $1.4765 \pm 0.006 \times 10^{22}$  kg from P1’s orbit.<sup>1</sup> The values of  $m_p + m_c$  from P2 and P1 disagree with that from Charon at the  $2.1\text{-}\sigma$  and  $3.2\text{-}\sigma$  levels, respectively. As we shall see, the discrepancies are in fact due to the deviation from Kepler’s third law for P2 and P1. Because of the rather large mass ratio of Charon-Pluto, the deviations of the gravitational potential from that of a point mass and, consequently, of the orbits of P2 and P1 from Keplerian orbits are nontrivial,

---

<sup>1</sup>We note that the masses reported by BGYYS are consistent with using  $G = 6.67 \times 10^{-11} \text{ m}^3 \text{ kg}^{-1} \text{ s}^{-2}$  instead of  $G = 6.672 \times 10^{-11} \text{ m}^3 \text{ kg}^{-1} \text{ s}^{-2}$  in converting from  $G(m_p + m_c) = (2\pi/P)^2 a^3$  to  $m_p + m_c$ .

even if P2 and P1 can be treated as test particles.

The second result from the orbit-fitting that suggests non-Keplerian orbits for P2 and P1 is the confirmation of the result of Weaver et al. (2006) that the orbital periods of Charon, P2, and P1 are nearly in the ratio 1:4:6. This means that the orbits of P2 and P1 could be strongly affected by resonant or near-resonant interactions. As we shall see, the strongest effects come from the proximity of P2 and P1 to the 3:2 mean-motion commensurability, which is the lowest order commensurability among the satellites, even though P2 and P1 are much smaller than Charon.

In Section 2 we present an analytic theory for the orbits of P2 and P1 that is valid in the limit that the satellites have negligible masses and can be treated as test particles. It shows that the motion can be represented by the superposition of the circular motion of a guiding center, the forced oscillations due to the non-axisymmetric components of the potential rotating at the mean motion of Pluto-Charon, the epicyclic motion, and the vertical motion. It also gives analytic results for the deviation from Kepler’s third law and the periape and nodal precession rates. In Section 3 we present direct numerical orbit integrations with different assumed masses for P2 and P1 within the ranges allowed by the uncertainties in the albedos. The numerical results are compared to the analytic theory in Section 2, and the increasing importance of the proximity to the 3:2 commensurability with increasing masses is examined. In fact, for the maximum masses corresponding to the lowest expected albedos, P2 and P1 may be in the 3:2 mean-motion resonance, with the resonance variable involving the periape longitude of P1 librating. In Section 4 we summarize our results and discuss the prospects for detecting non-Keplerian behaviors and putting constraints on the masses of P2 and P1 with existing and future observations.

## 2. ANALYTIC THEORY

In this section we develop an analytic theory for the orbits of the satellites P2 and P1 that is valid in the limit that the satellites have negligible masses and can be treated as test particles. The latest orbital fit show that the orbit of Charon relative to Pluto is consistent with zero eccentricity (see Table 1). Thus we assume that the orbit of Charon relative to Pluto is Keplerian and circular, with semimajor axis  $a_{pc}$  and mean motion (or circular frequency)  $n_{pc} = [G(m_p + m_c)/a_{pc}^3]^{1/2}$ , where  $m_p$  and  $m_c$  are the masses of Pluto and Charon, respectively. In a cylindrical coordinate system with the origin at the center of mass of the Pluto-Charon system and the  $z = 0$  plane being the orbital plane of Pluto-Charon, the positions of Charon and Pluto are  $\mathbf{r}_c = (a_c, \phi_c, 0)$ , and  $\mathbf{r}_p = (a_p, \phi_c + \pi, 0)$ , respectively, where  $a_p = a_{pc}m_c/(m_p + m_c)$ ,  $a_c = a_{pc}m_p/(m_p + m_c)$ ,  $\phi_c(t) = n_{pc}t + \varphi_{pc}$ , and  $\varphi_{pc}$  is a constant.

## 2.1. Potential

Since the orbital radii of the satellites are much smaller than the Hill radius ( $\approx 8.0 \times 10^6$  km) of the Pluto-Charon system, the perturbation from the Sun can be ignored and the gravitational potential at  $\mathbf{r} = (R, \phi, z)$  is

$$\Phi(\mathbf{r}) = -\frac{Gm_p}{|\mathbf{r} - \mathbf{r}_p|} - \frac{Gm_c}{|\mathbf{r} - \mathbf{r}_c|}. \quad (1)$$

The orbits of the satellites are nearly coplanar with that of Pluto-Charon, and we expand  $1/|\mathbf{r} - \mathbf{r}_c|$  in powers of  $z$ :

$$\frac{1}{|\mathbf{r} - \mathbf{r}_c|} = \frac{1}{(\rho^2 + z^2)^{1/2}} = \frac{1}{\rho} - \frac{1}{2} \frac{z^2}{\rho^3} + \dots, \quad (2)$$

where

$$\rho = [R^2 + a_c^2 - 2Ra_c \cos(\phi - \phi_c)]^{1/2}. \quad (3)$$

By expressing the inverse powers of  $\rho$  as cosine series using the Laplace coefficients (see Eq. [6.62] of Murray and Dermott 1999), we obtain

$$\frac{1}{|\mathbf{r} - \mathbf{r}_c|} = \frac{1}{2R} \sum_{k=0}^{\infty} (2 - \delta_{k0}) \left[ b_{1/2}^k(\alpha_c) - \frac{1}{2} \left( \frac{z}{R} \right)^2 b_{3/2}^k(\alpha_c) + \dots \right] \cos k(\phi - \phi_c), \quad (4)$$

where  $\delta_{k0}$  is the Kronecker delta,  $\alpha_c = a_c/R$ , and  $b_s^k(\alpha_c)$  are the Laplace coefficients. With a similar expression for  $1/|\mathbf{r} - \mathbf{r}_p|$ , the potential can be written as

$$\Phi(\mathbf{r}) = \sum_{k=0}^{\infty} \left[ \Phi_{0k}(R) - \frac{1}{2} \left( \frac{z}{R} \right)^2 \Phi_{2k}(R) + \dots \right] \cos k(\phi - \phi_c), \quad (5)$$

where

$$\Phi_{jk}(R) = -\frac{2 - \delta_{k0}}{2} \left[ \frac{m_c}{(m_p + m_c)} b_{(j+1)/2}^k(\alpha_c) + (-1)^k \frac{m_p}{(m_p + m_c)} b_{(j+1)/2}^k(\alpha_p) \right] \frac{G(m_p + m_c)}{R}. \quad (6)$$

The axisymmetric  $k = 0$  components of the potential are identical to those due to two rings — one of mass  $m_p$  and radius  $a_p$  and another of mass  $m_c$  and radius  $a_c$  — at the  $z = 0$  plane.

Since  $a_{pc}/R \approx 0.40$  and  $0.30$  for P2 and P1, respectively, it is instructive to examine the expansion of  $\Phi_{0k}$  in powers of  $a_{pc}/R$  for the lowest values of  $k$ :

$$\Phi_{00} = - \left[ 1 + \frac{1}{4(1 + m_c/m_p)^2} \left( \frac{m_c}{m_p} \right) \left( \frac{a_{pc}}{R} \right)^2 + \frac{9(1 - m_c/m_p + m_c^2/m_p^2)}{64(1 + m_c/m_p)^4} \left( \frac{m_c}{m_p} \right) \left( \frac{a_{pc}}{R} \right)^4 + \dots \right] \frac{G(m_p + m_c)}{R}, \quad (7)$$

$$\Phi_{01} = - \left[ \frac{3(1 - m_c/m_p)}{8(1 + m_c/m_p)^3} \left( \frac{m_c}{m_p} \right) \left( \frac{a_{pc}}{R} \right)^3 + \dots \right] \frac{G(m_p + m_c)}{R}, \quad (8)$$

$$\Phi_{02} = - \left[ \frac{3}{4(1 + m_c/m_p)^2} \left( \frac{m_c}{m_p} \right) \left( \frac{a_{pc}}{R} \right)^2 + \frac{5(1 - m_c/m_p + m_c^2/m_p^2)}{16(1 + m_c/m_p)^4} \left( \frac{m_c}{m_p} \right) \left( \frac{a_{pc}}{R} \right)^4 + \dots \right] \frac{G(m_p + m_c)}{R}, \quad (9)$$

$$\Phi_{03} = - \left[ \frac{5(1 - m_c/m_p)}{8(1 + m_c/m_p)^3} \left( \frac{m_c}{m_p} \right) \left( \frac{a_{pc}}{R} \right)^3 + \dots \right] \frac{G(m_p + m_c)}{R}, \quad (10)$$

and also the expansion of  $\Phi_{20}$ :

$$\Phi_{20} = - \left[ 1 + \frac{9}{4(1 + m_c/m_p)^2} \left( \frac{m_c}{m_p} \right) \left( \frac{a_{pc}}{R} \right)^2 + \frac{225(1 - m_c/m_p + m_c^2/m_p^2)}{64(1 + m_c/m_p)^4} \left( \frac{m_c}{m_p} \right) \left( \frac{a_{pc}}{R} \right)^4 + \dots \right] \frac{G(m_p + m_c)}{R}. \quad (11)$$

From the series definition of the Laplace coefficients (Eq. [6.68] of Murray and Dermott 1999), one expects the lowest order terms of  $\Phi_{jk}$  to be of the order of  $(a_{pc}/R)^k$ . However, the terms of the order of  $a_{pc}/R$  in  $\Phi_{01}$  cancel, and the lowest order nonzero terms in  $\Phi_{01}$  is of the order of  $(a_{pc}/R)^3$ . Eqs. (7) and (11) show that the axisymmetric components of the potential deviate from that of a point mass of mass  $m_p + m_c$  at the origin by terms of the order of  $(a_{pc}/R)^2$  and higher, while Eqs. (8)–(10) show that the non-axisymmetric components of the potential are weak and of the order of  $(a_{pc}/R)^2$  and higher. It should be noted that the deviations from a point mass potential are multiplied by an additional small quantity  $m_c/m_p$ .

## 2.2. Equations of Motion and Solution

The equations of motion in cylindrical coordinates are

$$\begin{aligned} \ddot{R} - R\dot{\phi}^2 &= -\frac{\partial\Phi}{\partial R}, \\ R\ddot{\phi} + 2\dot{R}\dot{\phi} &= -\frac{1}{R}\frac{\partial\Phi}{\partial\phi}, \\ \ddot{z} &= -\frac{\partial\Phi}{\partial z}. \end{aligned} \quad (12)$$

The gravitational potential  $\Phi$  (Eq. [5]) is weakly non-axisymmetric and rotates at a constant pattern speed  $n_{pc}$ , and the satellites P2 and P1 are on nearly circular orbits that are nearly coplanar with that of Pluto-Charon. An approximate solution to the equations of motion that is valid for such orbits can be obtained by representing the orbit as small deviations from the circular motion of a guiding center in the  $z = 0$  plane:

$$\begin{aligned} R &= R_0 + R_1(t), \\ \phi &= \phi_0(t) + \phi_1(t), \\ z &= z_1(t), \end{aligned} \quad (13)$$

where the constant  $R_0$  is the radius of the guiding center,  $|R_1/R_0| \ll 1$ ,  $|\phi_1| \ll 1$ , and  $|z_1/R_0| \ll 1$ . The approach is well known from the theory of orbits in weakly barred galaxies (see, e.g., Binney and Tremaine 1987) and planetary ring dynamics (see, e.g., Goldreich and Tremaine 1982).

Substituting Eqs. (5) and (13) into Eq. (12), the only nontrivial equation at the zeroth order is

$$R_0 \dot{\phi}_0^2 = \left[ \frac{d\Phi_{00}}{dR} \right]_{R_0}, \quad (14)$$

which describes the circular motion of the guiding center. The solution of Eq. (14) is

$$\phi_0(t) = n_0 t + \varphi_0, \quad (15)$$

where  $\varphi_0$  is a constant and the mean motion  $n_0$  is given by

$$n_0^2 = \left[ \frac{1}{R} \frac{d\Phi_{00}}{dR} \right]_{R_0} \quad (16)$$

$$= \frac{1}{2} \left\{ \frac{m_c}{(m_p + m_c)} b_{1/2}^0(\alpha_c) + \frac{m_p}{(m_p + m_c)} b_{1/2}^0(\alpha_p) \right. \\ \left. + \frac{m_p m_c}{(m_p + m_c)^2} \left( \frac{a_{pc}}{R_0} \right) \left[ D b_{1/2}^0(\alpha_c) + D b_{1/2}^0(\alpha_p) \right] \right\} n_K^2. \quad (17)$$

In the above equation  $n_K = [G(m_p + m_c)/R_0^3]^{1/2}$  is the Keplerian mean motion at  $R_0$ ,  $D = d/d\alpha$ , and  $\alpha_c$  and  $\alpha_p$  are evaluated at  $R = R_0$ .

At the first order, the equation for  $\phi_1$  is

$$\ddot{\phi}_1 + \frac{2n_0}{R_0} \dot{R}_1 = \sum_{k=1}^{\infty} \frac{k\Phi_{0k}(R_0)}{R_0^2} \sin(k\Delta\phi), \quad (18)$$

where

$$\Delta\phi = \phi_0 - \phi_c = (n_0 - n_{pc})t + \varphi_0 - \varphi_{pc}. \quad (19)$$

An integration of Eq. (18) yields an expression for  $\dot{\phi}_1$ , which can then be substituted into the first order equation for  $R_1$  to yield

$$\ddot{R}_1 + \kappa_0^2 R_1 = - \sum_{k=1}^{\infty} \left[ \frac{d\Phi_{0k}}{dR} + \frac{2n\Phi_{0k}}{R(n - n_{pc})} \right]_{R_0} \cos(k\Delta\phi), \quad (20)$$

where the epicyclic frequency  $\kappa_0$  is given by

$$\kappa_0^2 = \left[ R \frac{dn^2}{dR} + 4n^2 \right]_{R_0} \quad (21)$$

$$\begin{aligned}
= & \frac{1}{2} \left\{ \frac{m_c}{(m_p + m_c)} b_{1/2}^0(\alpha_c) + \frac{m_p}{(m_p + m_c)} b_{1/2}^0(\alpha_p) \right. \\
& - \frac{m_p m_c}{(m_p + m_c)^2} \left( \frac{a_{pc}}{R_0} \right) \left[ D b_{1/2}^0(\alpha_c) + D b_{1/2}^0(\alpha_p) \right] \\
& \left. - \frac{m_p m_c}{(m_p + m_c)^2} \left( \frac{a_{pc}}{R_0} \right)^2 \left[ \frac{m_p}{(m_p + m_c)} D^2 b_{1/2}^0(\alpha_c) + \frac{m_c}{(m_p + m_c)} D^2 b_{1/2}^0(\alpha_p) \right] \right\} n_K^2.
\end{aligned} \tag{22}$$

In Eqs. (20) and (21),  $n = (R^{-1} d\Phi_{00}/dR)^{1/2}$  is the mean motion at  $R$ , and the quantities in the square brackets are evaluated at  $R = R_0$ . Eq. (20) is the equation of motion of a simple harmonic oscillator of natural frequency  $\kappa_0$  that is driven at frequencies  $k|n_0 - n_{pc}|$ . It is straightforward to solve Eqs. (18) and (20) to obtain

$$R = R_0 \left[ 1 - e \cos(\kappa_0 t + \psi) + \sum_{k=1}^{\infty} C_k \cos(k\Delta\phi) \right], \tag{23}$$

$$\phi = n_0 t + \varphi_0 + \frac{2n_0}{\kappa_0} e \sin(\kappa_0 t + \psi) - \frac{n_0}{(n_0 - n_{pc})} \sum_{k=1}^{\infty} \frac{D_k}{k} \sin(k\Delta\phi), \tag{24}$$

$$\dot{R} = R_0 \left[ e\kappa_0 \sin(\kappa_0 t + \psi) - (n_0 - n_{pc}) \sum_{k=1}^{\infty} k C_k \sin(k\Delta\phi) \right], \tag{25}$$

$$\dot{\phi} = n_0 \left[ 1 + 2e \cos(\kappa_0 t + \psi) - \sum_{k=1}^{\infty} D_k \cos(k\Delta\phi) \right], \tag{26}$$

where  $e$  and  $\psi$  are constants,

$$C_k = - \left[ \frac{1}{R} \frac{d\Phi_{0k}}{dR} + \frac{2n\Phi_{0k}}{R^2(n - n_{pc})} \right]_{R_0} / \left[ \kappa_0^2 - k^2(n_0 - n_{pc})^2 \right], \tag{27}$$

and

$$D_k = 2C_k + \frac{\Phi_{0k}(R_0)}{R_0^2 n_0 (n_0 - n_{pc})}. \tag{28}$$

Finally, for the motion in  $z$ , the first order equation for  $z_1$  is

$$\ddot{z}_1 + \nu_0^2 z_1 = 0, \tag{29}$$

and its solution gives

$$z = z_1 = R_0 i \cos(\nu_0 t + \zeta) \tag{30}$$

where  $i$  and  $\zeta$  are constants and the vertical frequency  $\nu_0$  is defined by

$$\nu_0^2 = \left[ -\frac{\Phi_{20}}{R^2} \right]_{R_0} \tag{31}$$

$$= \frac{1}{2} \left[ \frac{m_c}{(m_p + m_c)} b_{3/2}^0(\alpha_c) + \frac{m_p}{(m_p + m_c)} b_{3/2}^0(\alpha_p) \right] n_K^2. \tag{32}$$

The motion in  $R$  and  $\phi$  is described by the superposition of the circular motion of the guiding center at  $R_0$  at frequency  $n_0$ , the epicyclic motion represented by “eccentricity”  $e$  at frequency  $\kappa_0$ , and the forced oscillations of fractional radial amplitudes  $C_k$  at frequencies  $k|n_0 - n_{pc}|$ . The motion in  $z$  decouples from that in  $R$  and  $\phi$  and has only free oscillations at the vertical frequency  $\nu_0$ . If there is no epicyclic or vertical motion ( $e = i = 0$ ), the orbit is a closed orbit in the frame rotating at the pattern speed  $n_{pc}$ , with the variation of the radius with the azimuthal angle being the sum of terms with fractional amplitude  $C_k$  and period  $2\pi/k$ . If  $e \gg \sum_k C_k$ , the orbit is approximately a precessing Keplerian ellipse with eccentricity  $e$ , mean motion  $n_0$ , and periape precession rate

$$\dot{\varpi} = n_0 - \kappa_0. \quad (33)$$

If in addition  $i \neq 0$ , the orbit has an inclination  $i$  with respect to the Pluto-Charon orbital plane and a nodal precession rate

$$\dot{\Omega} = n_0 - \nu_0. \quad (34)$$

### 2.3. Deviation from Kepler’s Third Law

Eq. (17) shows that the mean motion  $n_0$  and hence the azimuthal period  $P_0 = 2\pi/n_0$  deviate from those of a Keplerian orbit. In Fig. 1 the solid line shows  $P_K/P_0 - 1 = n_0/n_K - 1$  from Eq. (17) as a function of the guiding center radius  $R_0$  for the best-fit mass ratio of Charon-Pluto,  $m_c/m_p = 0.1165$ , while the dotted lines show the same quantity for  $m_c/m_p$  that are  $1\sigma$  ( $\pm 0.0055$ ) from the best-fit value. (The uncertainty in  $m_c/m_p$  dominates that in  $a_{pc}$  in the evaluation of Eq. [17].) Fig. 1 shows that the azimuthal period is shorter than the Keplerian orbital period.

The orbital parameters of P2 and P1 in Table 1 were obtained by BGYYS from unperturbed Keplerian fits. As we have shown in this section, the orbits of P2 and P1 are non-Keplerian even if they can be treated as test particles. Nevertheless, the orbital period  $P$  and semimajor axis  $a$  (which are independent parameters in the fits by BGYYS) in Table 1 should closely resemble the azimuthal period  $P_0$  and guiding center radius  $R_0$ . With  $P_K = 2\pi[a^3/G(m_p + m_c)]^{1/2} = P_{pc}(a/a_{pc})^{3/2}$ , where  $P_{pc}$  and  $a_{pc}$  are the orbital period and semimajor axis of Pluto-Charon from Table 1, we find  $P_K/P - 1 = 0.0079 \pm 0.0038$  and  $0.0067 \pm 0.0021$  for P2 and P1, respectively. The values of  $P_K/P - 1$  and  $a$  for P2 and P1 are shown in Fig. 1 with their  $1\sigma$  error bars. The orbital periods are clearly shorter than the Keplerian values (by  $2.1\sigma$  and  $3.2\sigma$  for P2 and P1, respectively). On the other hand,  $P_K/P - 1$  for P2 is in excellent agreement (within  $0.4\sigma$ ) with the analytic result, and that for P1 is in reasonable agreement (within  $1.6\sigma$ ) with the analytic result. The remaining discrepancy for P1 may be simply statistical, but it could also be due to the assumption in the fitting that the orbit is an unperturbed Keplerian orbit (see below for more details on the expected non-Keplerian behaviors).



## 2.4. Periapse and Nodal Precessions

With  $a$  from Table 1 as  $R_0$  for P2 and P1 and  $m_c/m_p = 0.1165$ , we evaluate  $P_K = P_{pc}(a/a_{pc})^{3/2}$ ,  $n_0/n_K$  (Eq. [17]),  $\kappa_0/n_K$  (Eq. [22]), and  $\nu_0/n_K$  (Eq. [32]) for the analytic theory, and they are listed in Table 2. The precession of the periapse is prograde with period  $2\pi/|\dot{\varpi}| = 2\pi/|n_0 - \kappa_0| = 1740$  and 5280 days for P2 and P1, respectively. The nodal precession has a similar period ( $2\pi/|\dot{\Omega}| = 2\pi/|n_0 - \nu_0| = 1770$  and 5330 days for P2 and P1, respectively) but it is retrograde.

The periapse and nodal precessions at nearly equal rates in opposite directions and the faster-than-Keplerian mean motion are similar to the behaviors of orbits around an oblate planet (see, e.g., Section 6.11 of Murray and Dermott 1999). This can be understood from the fact that the  $(a_{pc}/R)^2$  terms in the axisymmetric components of the potential,  $\Phi_{00}$  and  $\Phi_{20}$  in Eqs. (7) and (11), are identical to the  $J_2$  terms of an oblate planet with  $J_2 = m_p m_c / [2(m_p + m_c)^2]$ .

## 3. NUMERICAL ORBIT INTEGRATIONS

### 3.1. Initial Conditions and Numerical Methods

For the remainder of this paper we use Jacobi coordinates where the position of Charon is relative to Pluto, the position of the inner satellite P2 is relative to the center of mass of Pluto-Charon, and the position of the outer satellite P1 is relative to the center of mass of Pluto-Charon-P2. Jacobi coordinates are the natural generalization of the coordinates used in Section 2 (where the position of P1 is relative to the center of mass of Pluto-Charon) when P2 and P1 are not test particles, and they reduce to the coordinates used in Section 2 in the test-particle limit.

From  $P_{pc}$  and  $a_{pc}$  in Table 1, we adopt  $G(m_p + m_c) = (2\pi/P_{pc})^2 a_{pc}^3 = 9.71791 \times 10^{11} \text{ m}^3 \text{ s}^{-2}$  (or  $m_p + m_c = 1.4565 \times 10^{22} \text{ kg}$  for  $G = 6.672 \times 10^{-11} \text{ m}^3 \text{ kg}^{-1} \text{ s}^{-2}$ ). For the mass ratio  $m_c/m_p$ , we use the best-fit value 0.1165 from BGYYS. We generate the initial position and velocity of Charon relative to Pluto by using the orbital parameters in Table 1 at epoch JD 2452600.5 as the osculating Keplerian orbital parameters.

The orbits of P2 and P1 are sufficiently non-Keplerian even in the test-particle limit that, if we had generated their initial conditions by assuming that the orbital parameters in Table 1 are the osculating Keplerian parameters at epoch JD 2452600.5, the numerically integrated orbits would have properties significantly different from those of the best-fit Keplerian orbits in Table 1, with the mean orbital radii smaller than the semimajor axes in Table 1 and the variations in the orbital radii larger than those for the eccentricities in Table 1. Without refitting the data, we aim to adopt a set of initial conditions so that the resulting orbits would closely resemble the best-fit Keplerian orbits in Table 1. This is accomplished by using the mean longitudes  $\lambda$  of P2 and P1 in Table 1 as the initial values of  $\phi$  and then using Eqs. (23), (25), and (26) to set the initial values of  $R$ ,  $\dot{R}$ , and  $\dot{\phi}$ . As in Sections 2.3–2.4, we adopt the semimajor axes  $a$  from the Keplerian fit as the guiding center radii  $R_0$ . We include the forced oscillation terms up to  $k = 4$ , and the coefficients  $C_k$  and

$D_k$  are listed in Table 2, along with  $P_K$ ,  $n_0/n_K$ ,  $\kappa_0/n_K$ , and  $\nu_0/n_K$ . For the initial values of  $\Delta\phi$  in the forced oscillation terms, we can ignore the difference between  $\phi$  and  $\phi_0$  (with the latter for the guiding center) and use  $\phi - \phi_c$ .

We can see from Table 2 that  $\sum_k C_k \approx 0.0029$  for P2. Thus the fractional orbital radius variation due to the forced oscillation terms alone is comparable to that due to the best-fit Keplerian eccentricity (0.0023), which is itself consistent with zero ( $\pm 0.0021$ ). Therefore, we set the initial epicyclic eccentricity  $e = 0$  for P2. For P1,  $\sum_k C_k \approx 0.0004$ , which is much smaller than the best-fit Keplerian eccentricity of 0.0052 ( $\pm 0.0011$ ), and we adopt an initial epicyclic eccentricity  $e = 0.0052$ . In the epicyclic approximation for a Keplerian orbit, the phase  $\kappa_0 t + \psi$  is the mean anomaly. So it is reasonable to adopt for P1  $\psi = \lambda - \varpi$ , where  $\lambda$  and  $\varpi$  are the mean longitude and longitude of periaapse from Table 1.

BGYYS have computed the 1- $\sigma$  contours of the orbit poles on the J2000 sky plane for their best-fit Keplerian orbits for Charon, P2, and P1 using the Monte Carlo technique, and the contours are shown in their Fig. 2. The 1- $\sigma$  contour for Charon is significantly smaller than those for P2 and P1, with the latter two having mean radii of about 0°34 and 0°16, respectively. The orbit pole of Charon is 0°10 from that of P2 for the best-fit orbits, which is well within the 1- $\sigma$  contour for P2, and it is 0°25 from that of P1 for the best-fit orbits, which is about 50% further than the 1- $\sigma$  contour for P1 and only marginally significant. Since there is no significant detection of any mutual orbital inclinations, we assume that the orbits of P2 and P1 are coplanar with that of Pluto-Charon. This means that the precession of nodes is not examined by our numerical orbit integrations.

We perform 5 sets of integrations with different assumed masses for P2 and P1. From the photometry of P2 and P1, Weaver et al. (2006) have estimated that the diameters of P2 and P1 are  $46 \pm 4$  km and  $61 \pm 4$  km, respectively, if the geometric albedos are Charon-like and = 0.35. On the other hand, if the albedos are comet-like and = 0.04, the diameters are  $137 \pm 11$  km for P2 and  $167 \pm 10$  km for P1. If we assume that the mean density is  $2 \text{ g cm}^{-3}$  (i.e., similar to that of Pluto),  $m_2 = 1.02 \times 10^{17}$  kg and  $m_1 = 2.38 \times 10^{17}$  kg in the high albedo case, and  $m_2 = 2.69 \times 10^{18}$  kg and  $m_1 = 4.88 \times 10^{18}$  kg in the low albedo case. In addition to two integrations with the high- and low-albedo masses, we perform an integration with masses  $10^{-5}$  times those of the high albedo case (so that P2 and P1 are test particles), an integration with masses twice those of the high albedo case, and an integration with masses half those of the low albedo case.

The direct numerical orbit integrations are performed using a modified version of the Wisdom and Holman (1991) symplectic integrator contained in the SWIFT<sup>2</sup> software package. The Wisdom-Holman integrator is based on dividing the Hamiltonian of the gravitational  $N$ -body problem into a part that describes the Keplerian motions of the satellites around the planet (or, in the case of a planetary system, the planets around the star) and a part that describes the perturbations to

---

<sup>2</sup>See <http://www.boulder.swri.edu/~hal/swift.html>.

the Keplerian motions. The division used by Wisdom and Holman (1991) assumes that all of the satellite masses are much smaller than the planet mass, but in the case of Pluto,  $m_c/m_p = 0.1165$ . We have described in Lee and Peale (2003) a modified Wisdom-Holman integrator using a slightly different division of the Hamiltonian into the Keplerian and perturbation parts. The modified integrator is designed for hierarchical systems, where the masses of the satellites can be comparable to that of the planet but the orbit of each satellite is much larger than that of the satellite just inside, and it was used by Lee and Peale (2003) to study hierarchical extrasolar planetary systems. This modified integrator can also handle the Pluto system, where  $(m_c/m_p)(a_{pc}/R)^2 \lesssim 0.019$ , without an excessively small timestep. The integrations are performed with a timestep of  $10^4$  s (or about 55 steps per Charon’s orbit).

### 3.2. Results

The numerical orbit integrations with test-particle masses, high-albedo masses, and twice the high-albedo masses for P2 and P1 show that the orbits of P2 and P1 are well described by the analytic theory in Section 2 if the masses of P2 and P1 are of the order of the high albedo ones. In Fig. 2 we plot the variations in the orbital radii  $R_2$  and  $R_1$  of P2 and P1, respectively, for 800 days in the high albedo case. The dashed lines indicate the semimajor axes,  $a$ , and the maximum and minimum radii,  $a(1 \pm e)$ , for the best-fit Keplerian orbits in Table 1. The orbital radius  $R_2$  of P2 clearly shows the forced oscillations, which are dominated by the  $C_1$  and  $C_2$  terms (see Table 2) with periods  $2\pi/|n_0 - n_{pc}| \approx 8.6$  days and  $\pi/|n_0 - n_{pc}| \approx 4.3$  days, respectively. As expected, the variation in  $R_2$  due to the forced oscillations is comparable in magnitude to that due to the best-fit Keplerian eccentricity. Although the initial epicyclic eccentricity of P2 is set to zero, the fact that the forced oscillation terms with  $k > 4$  are not included in setting the initial conditions results in a small epicyclic motion with a period  $2\pi/\kappa_0 \approx 25.2$  days, which is also visible in the plot of  $R_2$  in Fig. 2. The variation in  $R_1$  is dominated by the epicyclic motion with  $e \approx 0.0052$  and period  $2\pi/\kappa_0 \approx 38.6$  days. For P1, the amplitudes of the forced oscillations are significantly smaller than for P2, as we expect from the values of  $C_k$  in Table 2, and the dominant forced oscillation periods are  $2\pi/|n_0 - n_{pc}| \approx 7.7$  days and  $\pi/|n_0 - n_{pc}| \approx 3.8$  days. The  $k > 4$  terms are sufficiently small for P1 that their neglect in the initial conditions do not result in any significant additional epicyclic motion.

In order to study in more detail the epicyclic component of the motion, we need to eliminate the high frequency forced oscillations. We find that the forced oscillations are sufficiently close to those predicted by the analytic theory in all of our numerical integrations that they can be effectively eliminated by defining a transformed orbital radius:

$$R' = R - R_0 \sum_k C_k \cos[k(\phi - \phi_c)], \quad (35)$$

with  $R_0$  and  $C_k$  from Table 2 and  $\phi$  and  $\phi_c$  from the numerical integrations themselves (compare to Eq. [23]). In Fig. 3 we plot the variations in  $R'_2$  and  $R'_1$  in the high albedo case, and it is clear

from a comparison with Fig. 2 that most of the forced oscillations are eliminated. Fig. 3 shows that there are small periodic variations in the maximum and minimum values of  $R'_2$  and  $R'_1$ , or equivalently in the epicyclic eccentricities  $e_2$  and  $e_1$ , in this run with the high-albedo masses. The amplitudes of the eccentricity variations are larger in the run with twice the high-albedo masses, while the eccentricities are nearly constant in the run with test-particle masses, which indicate that the variations are due to interactions between P2 and P1 (see below for more details).

The azimuthal period  $P_0$  can be determined for the numerical integrations from the cumulative increase in  $\phi$ . We find  $P_0 = 24.913$  and  $38.335$  days for P2 and P1, respectively, for the run with high-albedo masses, and they are identical to  $P_0$  found for the run with test-particle masses.<sup>3</sup> If we use  $P_K$  from Table 2,  $n_0/n_K = P_K/P_0 = 1.0056$  and  $1.0033$  for P2 and P1, respectively. The latter is in excellent agreement with the analytic value in Table 2, but the former is slightly smaller than the analytic value. The small discrepancy for P2 is due to the fact that the numerically integrated orbit has a non-zero epicyclic eccentricity, with P2 near the periaipse at  $t = 0$  (see Fig. 3), which means that the guiding center radius of the numerically integrated orbit ( $R_0 = 48698$  km from the average of the maximum and minimum values of  $R'_2$ ) is slightly larger than the value we were aiming for ( $R_0 = 48675$  km). (For P1, the guiding center radius of the numerically integrated orbit is identical to the value we were aiming for.) If we use  $P_K = 25.0695$  days for the numerically determined  $R_0$  instead of  $P_K = 25.0518$  days from Table 2 for P2, we find  $n_0/n_K = P_K/P_0 = 1.0063$ , which is in excellent agreement with the analytic value in Table 2 (note that the ratio  $n_0/n_K$  is much less sensitive to a small change in  $R_0$  than  $P_K$  and  $P_0$  separately).

The easiest way to determine the longitude of periaipse  $\varpi$  of the epicyclic motion as a function of time is to monitor the transformed orbital radius  $R'$  (Eq. [35]) during the numerical orbit integration. When  $R'$  changes from decreasing in a previous timestep to increasing in the current timestep, the satellite has passed the periaipse, and we can use the values of  $R'$  and  $\phi$  at the end of the current step and two previous steps to find the time of periaipse passage and  $\varpi$  ( $= \phi$  at the time of periaipse passage) by interpolation. Similarly, the time at which  $\varpi = \phi + 180^\circ$  (i.e., apoapse passage) can be determined. Fig. 4 shows the evolution of  $\varpi_2$  and  $\varpi_1$  of P2 and P1, respectively, for  $10^4$  days in the high albedo case. There are some spurious points in the plot of  $\varpi_2$ , because the forced oscillations are not perfectly eliminated in the transformed orbital radius and there are occasional false minima and maxima in  $R'_2$  when the epicyclic eccentricity  $e_2$  is very small (see Fig. 3). In this high albedo case, the long-term evolution of  $\varpi_2$  and  $\varpi_1$  are prograde precessions with periods of 2000 and 5300 days, respectively. The latter is in excellent agreement with the analytic result in Section 2.4, but the former is about 15% longer. The 15% discrepancy

---

<sup>3</sup>It should be recalled that we adopt the best-fit semi-major axes  $a$  from the Keplerian fit as the guiding center radii  $R_0$  and that the  $1\text{-}\sigma$  error in  $a$  is  $\pm 121$  km for P2 and  $\pm 88$  km for P1 (see Table 1). If we vary the guiding center radii by  $\pm 1\sigma$  in the initial conditions of our numerical integrations, we would find  $P_0 = 24.913 \pm 0.093$  and  $38.335 \pm 0.078$  days for P2 and P1, respectively. Thus, similar to the analytic results in Section 2.3, the azimuthal periods from the numerical integrations agree with the best-fit orbital periods in Table 1 from the Keplerian fit to within  $0.6\sigma$  for P2 and  $1.6\sigma$  for P1.

for P2 is too large to be explained by the slightly larger guiding center radius mentioned in the previous paragraph, and it is not due to interactions between P2 and P1, as the test-particle run shows the same precession period. We suspect that the discrepancy is due to the neglect of second (and higher) order corrections to the deviations from the guiding center motion in the analytic theory in Section 2.

Superposed on the long-term periapse precessions are periodic variations on the same timescales ( $\approx 400$  and  $450$  days for P2 and P1, respectively) as the epicyclic eccentricity variations seen in Fig. 3. For P2, the amplitude of the short-term variation is sufficiently large that the precession is retrograde when the eccentricity is large and prograde and faster than the long-term rate when the eccentricity is small. The short-term periodic variations in the epicyclic eccentricities and periapse longitudes are due to interactions between P2 and P1, and we can explain the periods by noting that their orbits are close to the 3:2 mean-motion commensurability (azimuthal period ratio = 1.539 for the numerical integration, in agreement with the ratio 1.537 for the best-fit orbital periods in Table 1). The disturbing potential for the interactions between P2 and P1, which is not included in the analytic theory in Section 2, can be expanded into a cosine series in the usual manner (see, e.g., Murray and Dermott 1999), and because of the proximity to the 3:2 commensurability, we expect the interactions to be dominated by the terms in the disturbing potential associated with the cosine arguments (or resonance variables)  $\theta_2 = 2\phi_2 - 3\phi_1 + \varpi_2$  and  $\theta_1 = 2\phi_2 - 3\phi_1 + \varpi_1$ .<sup>4</sup> Fig. 5 shows the evolution of  $\theta_2$  and  $\theta_1$  for  $10^4$  days in the high albedo case. It is clear from Fig. 5 that neither  $\theta_2$  nor  $\theta_1$  is in resonance and that the circulation periods of  $\theta_2$  and  $\theta_1$  are  $\approx 400$  and  $450$  days, respectively. Thus the short-term periodic variations in  $e_2$  and  $\varpi_2$  are associated with the circulation of  $\theta_2$  and those in  $e_1$  and  $\varpi_1$  are associated with the circulation of  $\theta_1$ .

The amplitudes of the short-term variations in  $e$  and  $\varpi$  are larger for *both* P2 and P1 for larger masses of P2 and P1, as long as the masses do not exceed about half the low-albedo ones. In the run with half the low-albedo masses (Figs. 6 and 7),  $e_1$  and  $\varpi_1$  show significant variations, with the minimum  $e_1$  much smaller than the initial  $e_1 = 0.0052$ . Both  $\varpi_2$  and  $\varpi_1$  alternate between nearly linear retrograde precession when the eccentricities are large and very fast prograde precession when the eccentricities are small. However, the long-term trends of both  $\varpi_2$  and  $\varpi_1$  remain prograde, with periods of 1900 and 5100 days, respectively, which are slightly shorter than in the case with the high-albedo masses.

In the run with the low-albedo masses (Figs. 8 and 9), while the properties of the orbit of P2 follow the same trends with increasing masses as above (i.e., larger amplitudes for the short-term variations of  $e_2$  and  $\varpi_2$  and a shorter period of 1800 days for the long-term prograde precession of  $\varpi_2$ ), those of P1 do not follow the previous trends. The amplitude of the variation in  $e_1$  is now smaller than in the case with half the low-albedo masses, and  $\varpi_1$  shows a completely retrograde

---

<sup>4</sup>For convenience, we define the resonance variables  $\theta_2$  and  $\theta_1$  using the true longitudes  $\phi_2$  and  $\phi_1$  instead of mean longitudes. While it is possible to define a mean longitude via a mean anomaly that is proportional to  $n_0 t$ , it cannot be easily computed from the position and velocity.

precession with a period of 500 days. The explanation can be found in the plot of the evolution of the resonance variables  $\theta_2$  and  $\theta_1$  in Fig. 10. While  $\theta_2$  circulates as in the high albedo case shown in Fig. 5 (the nearly empty region about  $180^\circ$  is due to the fast prograde precession of  $\varpi_2$  when  $e_2$  is small),  $\theta_1$  librates about  $180^\circ$ . Thus the case with the low-albedo masses differs from the cases with lower masses in having  $\theta_1$  in resonance.

#### 4. DISCUSSION AND CONCLUSIONS

We have analyzed the orbits of the recently discovered satellites of Pluto, S/2005 P1 and S/2005 P2. Because of the rather large mass ratio of Charon-Pluto ( $m_c/m_p \sim 0.1$ ), the orbits of P2 and P1 are non-Keplerian even if P2 and P1 have negligible masses. The analytic theory in Section 2 with P2 and P1 treated as test particles shows that the motion in  $R$  and  $\phi$  can be described by the superposition of the circular motion of the guiding center at mean motion  $n_0$ , the epicyclic motion represented by eccentricity  $e$  at epicyclic frequency  $\kappa_0$ , and the forced oscillations at frequencies  $k|n_0 - n_{pc}|$  ( $k = 1, 2, 3, \dots$ ) due to the non-axisymmetric components of the gravitational potential rotating at the mean motion  $n_{pc}$  of Pluto-Charon; the motion in  $z$  at the vertical frequency  $\nu_0$  decouples from that in  $R$  and  $\phi$ . With  $\nu_0 > n_0 > n_K > \kappa_0$ , where  $n_K$  is the Keplerian mean motion about the center of mass of Pluto and Charon, we found that the azimuthal period  $P_0 = 2\pi/n_0$  is shorter than the Keplerian orbital period and that the periaapse and ascending node (relative to the Pluto-Charon orbital plane) precess at nearly equal rates in opposite directions (prograde for the periaapse and retrograde for the node). We have also performed a series of direct numerical orbit integrations with different assumed masses for P2 and P1, and the results presented in Section 3 show the increasing effects of the proximity of the orbits of P2 and P1 to the 3:2 mean-motion commensurability with increasing masses. As shown in Fig. 1, the deviation from Kepler’s third law is already detected in the unperturbed Keplerian fit of BGYYS (which was previously pointed out by BGYYS as discrepancies in the total mass of Pluto-Charon inferred from the orbits of Charon, P2, and P1). Since the other non-Keplerian behaviors depend on the masses of P2 and P1, a dynamical fit to the data that accounts for the interactions among Charon, P2, and P1 should allow us to place constraints on the masses of P2 and P1, although the existing data consisting of only 12 observations over a 1-year time span may not be sufficient. (BGYYS included in their unperturbed Keplerian fits the discovery data for P2 and P1 from Weaver et al. 2006, which were taken two years after the last observation of BGYYS, but the discovery data have larger errors and may not be useful in constraining parameters other than the orbital periods.)

If the albedos of P2 and P1 are high and of order of that of Charon, the masses of P2 and P1 are sufficiently low that their orbits are well described by the analytic theory. The largest correction due to the proximity to the 3:2 commensurability is a significant variation of the precession of  $\varpi_2$  on the period of circulation ( $\approx 400$  days) of the resonance variable  $\theta_2 = 2\phi_2 - 3\phi_1 + \varpi_2$  (Figs. 4 and 5). However, the variation in the orbital radius  $R_2$  of P2 due to the forced oscillations are large (Fig. 2), and the eccentricity with a large error ( $0.0023 \pm 0.0021$ ) found by the Keplerian fit

of BGYYS probably results from an attempt to fit the 12 data points without taking into account the forced oscillations. Thus, there is at present no evidence that P2 has any significant epicyclic eccentricity, and it is likely that the periapse precession of P2 would be difficult to measure. On the other hand, the orbit of P1 has a significant epicyclic eccentricity. Over the 1-year time span of the existing data, the prograde precession of  $\varpi_1$  with a period of 5300 days (Fig. 4) would have resulted in a  $25^\circ$  change in  $\varpi_1$ , which may be difficult to detect with only 12 data points. But there would be more than 3.6 yr between the first existing data point and any additional data of comparable quality taken after the writing of this paper (Feb. 2006), and the  $\gtrsim 90^\circ$  precession of  $\varpi_1$  should be detectable.

If the albedos of P2 and P1 are low and of order of that of comets, the masses of P2 and P1 are sufficiently large that there are significant short-term variations in their epicyclic eccentricities and/or periapse longitudes due to the proximity to the 3:2 commensurability. In the case with half the low-albedo masses (Figs. 6 and 7), there are significant variations in  $e_2$  and  $\varpi_2$  on the circulation period of  $\approx 400$  days of  $\theta_2$ , and in  $e_1$  and  $\varpi_1$  on the circulation period of  $\approx 450$  days of  $\theta_1 = 2\phi_2 - 3\phi_1 + \varpi_1$ . In the case with low-albedo masses (Figs. 8, 9, and 10),  $\theta_1$  is in resonance and  $\varpi_1$  shows a retrograde precession with a period of only 500 days. Since the existing data can be reasonably fitted by unperturbed Keplerian orbits, one might speculate that the existing data are already inconsistent with masses of P2 and P1 near the upper end of the expected range. But we cannot rule out the possibility that orbits like those in Figs. 6–9 can be fitted by Keplerian orbits, if the orbits are sparsely sampled as in the existing data set. Another indication that masses of P2 and P1 near the upper end of the expected range may already be ruled out comes from the orbital eccentricity,  $e_c$ , of Charon. As pointed out by Stern et al. (1994), the perturbations from additional satellites in the Pluto-Charon system induce eccentricity in Charon’s orbit, and the observed value or upper limit of  $e_c$  can be used to constrain the masses of the additional satellites. In Fig. 11 we show the variation of  $e_c$  for 800 days in the run with low-albedo masses. The eccentricity  $e_c$  varies up to  $2 \times 10^{-4}$ , which is significantly larger than the best-fit  $e_c = 0.0 \pm 7.0 \times 10^{-5}$  in Table 1. But it should be noted that the random error of  $7.0 \times 10^{-5}$  corresponds to shifts of the order of 0.1 mas in the positions of Charon relative to Pluto, and it is unclear that systematic error in, e.g., the correction from the center of light to the center of body is below 0.1 mas. In any case, a data set that samples more densely any possible variations in the orbits of P2 and P1 on the 400-500-day timescales should provide strong constraints on the masses of P2 and P1.

There are no apparent effects due to the respective proximity of P2 and P1 to the high-order 4:1 and 6:1 mean-motion commensurabilities with Charon. However, Ward and Canup (2006) have proposed that P2 and P1 may have been trapped in the corotation resonances at these commensurabilities (i.e., those associated with the resonance variable  $\phi_c - 4\phi_2 + 3\varpi_c$  for P2 and  $\phi_c - 6\phi_1 + 5\varpi_c$  for P1) during the tidal expansion of Charon’s orbit, if Charon formed with large orbital eccentricity from a giant impact on Pluto. P2 and P1 escaped from the corotation resonances when Charon’s orbital eccentricity was tidally damped to very small value.

Our analysis shows that continued observations of the Pluto system with HST (and possibly

ground-based adaptive optics) in the near future will allow us to detect the non-Keplerian behaviors of the orbits of P2 and P1 (in addition to the already detected deviation from Kepler's third law) and to thereby constrain their masses. Much more precise determination of the orbits and masses of P2 and P1 will be possible as the New Horizons spacecraft approaches the Pluto system in 2015.

We thank Robin Canup and Alan Stern for sending us preprints on the new satellites of Pluto. This research was supported in part by NASA grant NNG05GK58G.



## REFERENCES

- Binney, J., Tremaine, S., 1987. *Galactic Dynamics*. Princeton Univ. Press, Princeton, Ch. 3.
- Buie, M. W., Grundy, W. M., Young, E. F., Young, L. A., Stern, S. A., 2006. Orbits and photometry of Pluto’s satellites: Charon, S/2005 P1 and S/2005 P2. *Astron. J.*, in press (astro-ph/0512491) (BGYY5).
- Christy, J. W., Harrington, R. S., 1978. The satellite of Pluto. *Astron. J.* 83, 1005–1008.
- Goldreich, P., Tremaine, S., 1982. The dynamics of planetary rings. *Ann. Rev. Astron. Astrophys.* 20, 249–283.
- Lee, M. H., Peale, S. J., 2003. Secular evolution of hierarchical planetary systems. *Astrophys. J.* 592, 1201–1216.
- Murray, C. D., Dermott, S. F., 1999. *Solar System Dynamics*. Cambridge Univ. Press, Cambridge.
- Sicardy, B., 44 colleagues, 2006. Charon’s size and an upper limit on its atmosphere from a stellar occultation. *Nature* 439, 52–54.
- Steffl, A. J., Mutchler, M. J., Weaver, H. A., Stern, S. A., Durda, D. D., Terrell, D., Merline, W. J., Young, L. A., Young, E. F., Buie, M. W., Spencer, J. R., 2006. New constraints on additional satellites of the Pluto system. *Astron. J.*, submitted (astro-ph/0511837).
- Stern, S. A., Parker, J. W., Duncan, M. J., Snowdall, J. C., Jr., Levison, H. F., 1994. Dynamical and observational constraints on satellites in the inner Pluto-Charon system. *Icarus* 108, 234–242.
- Tholen, D. J., Buie, M. W., 1997. The orbit of Charon. *Icarus* 125, 245–260.
- Ward, W. R., Canup, R. M., 2006. Forced resonant migration of Pluto’s outer satellites by an impact-produced Charon. *Science*, submitted.
- Weaver, H. A., Stern, S. A., Mutchler, M. J., Steffl, A. J., Buie, M. W., Merline, W. J., Spencer, J. R., Young, E. F., Young, L. A., 2006. Discovery of two new satellites of Pluto. *Nature* 439, 943–945.
- Wisdom, J., Holman, M., 1991. Symplectic maps for the n-body problem. *Astron. J.* 102, 1528–1538.

Table 1. Orbital Parameters at Epoch JD 2452600.5 from Keplerian fits by Buie et al. (2006)

Parameter	Charon	S/2005 P2	S/2005 P1
Period $P$ (days)	6.3872304(11)	24.8562(13)	38.2065(14)
Semimajor Axis $a$ (km)	19571.4(4.0)	48675(121)	64780(88)
Eccentricity $e$	0.000000(70)	0.0023(21)	0.0052(11)
Inclination $i$ (deg)	96.145(14)	96.18(22)	96.36(12)
Long. Ascending Node $\Omega$ (deg)	223.046(14)	223.14(23)	223.173(86)
Long. Periapse $\varpi$ (deg)	...	216(13)	200.1(3.7)
Mean Long. at Epoch $\lambda$ (deg)	257.946(13)	123.14(20)	322.71(23)

Note. — The parameters are for the orbit of Charon relative to Pluto and the orbits of P1 and P2 relative to the center of mass of Pluto-Charon. Numbers in parentheses are  $1\sigma$  errors in the least significant digits.

Table 2. Parameters of Analytic Theory

Parameter	S/2005 P2	S/2005 P1
$R_0$ (km)	48675	64780
$P_K = 2\pi/n_K$ (days)	25.0518	38.4628
$n_0/n_K$	1.00635	1.00341
$\kappa_0/n_K$	0.99198	0.99612
$\nu_0/n_K$	1.02053	1.01063
$C_1$	0.001275	0.000149
$C_2$	0.001373	0.000228
$C_3$	0.000204	0.000026
$C_4$	0.000044	0.000004
$D_1$	0.003220	0.000458
$D_2$	0.006813	0.001764
$D_3$	0.001496	0.000314
$D_4$	0.000437	0.000072

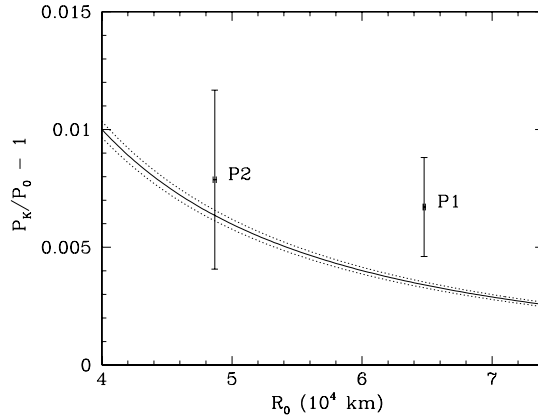


Fig. 1.— Deviation of azimuthal period  $P_0$  from Keplerian orbital period  $P_K$  as a function of the guiding center radius  $R_0$ . The solid line shows  $P_K/P_0 - 1 = n_0/n_K - 1$  from Eq. (17) for the best-fit mass ratio of Charon-Pluto,  $m_c/m_p = 0.1165$ , while the dotted lines show the same quantity for  $m_c/m_p$  that are  $1\sigma$  ( $\pm 0.0055$ ) from the best-fit value. The values of  $P_K/P - 1$  and  $a$  for the satellites P2 and P1, with orbital periods  $P$  and semimajor axes  $a$  from unperturbed Keplerian fits (Table 1), are shown with their  $1\sigma$  error bars.

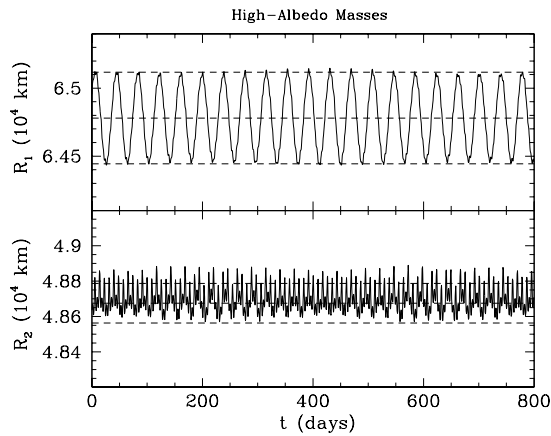


Fig. 2.— Variations in the orbital radii  $R_2$  and  $R_1$  of P2 and P1, respectively, for 800 days in the numerical orbit integration with the high-albedo masses for P2 and P1. The dashed lines indicate the semimajor axes,  $a$ , and the maximum and minimum radii,  $a(1 \pm e)$ , for the best-fit Keplerian orbits in Table 1. The variation in  $R_2$  is dominated by high-frequency forced oscillations due to the non-axisymmetric components of the potential rotating at the mean motion of Pluto-Charon, but a small epicyclic motion with period  $\approx 25.2$  days is also visible. The variation in  $R_1$  is dominated by the epicyclic motion with eccentricity  $\approx 0.0052$  and period  $\approx 38.6$  days.

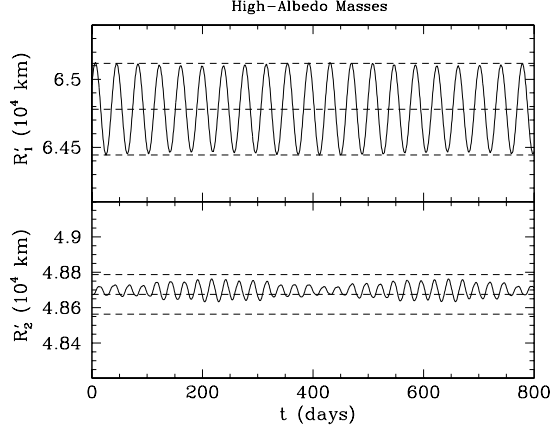


Fig. 3.— Same as Fig. 2, but for the transformed orbital radii  $R'_2$  and  $R'_1$  (Eq. [35]). Most of the forced oscillations in  $R_2$  and  $R_1$  are eliminated, and small periodic variations in the maximum and minimum values of  $R'_2$  and  $R'_1$ , or equivalently in the epicyclic eccentricities  $e_2$  and  $e_1$ , become visible. The periods are about 400 days for  $e_2$  and 450 days for  $e_1$ .

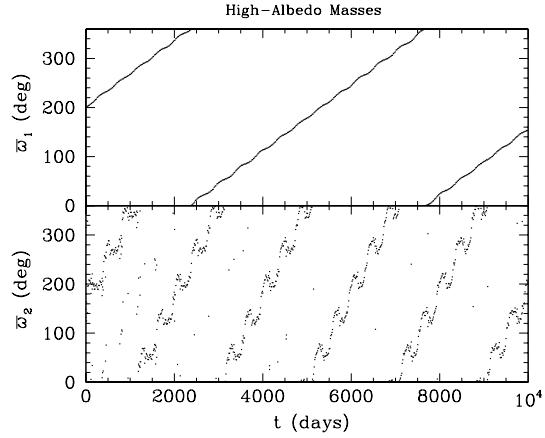


Fig. 4.— Evolution of the longitudes of periastron  $\varpi_2$  and  $\varpi_1$  of P2 and P1, respectively, for  $10^4$  days in the high albedo case. There are short-term periodic variations on the same timescales as  $e_2$  and  $e_1$ , but the long-term evolution is prograde precessions with periods of 2000 days for P2 and 5300 days for P1.

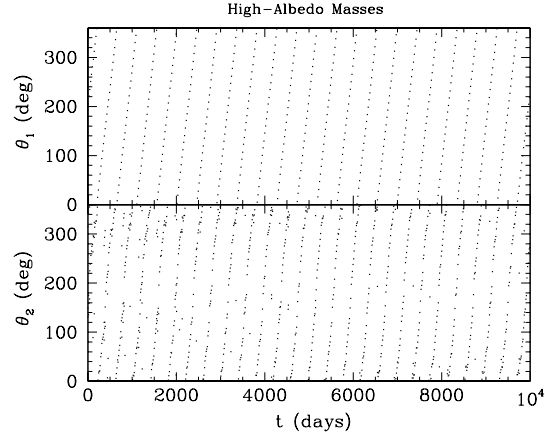


Fig. 5.— Same as Fig. 4, but for the resonance variables  $\theta_2 = 2\phi_2 - 3\phi_1 + \varpi_2$  and  $\theta_1 = 2\phi_2 - 3\phi_1 + \varpi_1$  at the 3:2 commensurability between P2 and P1. The period of the short-term variations in  $e_2$  and  $\varpi_2$  ( $e_1$  and  $\varpi_1$ ) is the circulation period of  $\theta_2$  ( $\theta_1$ ).

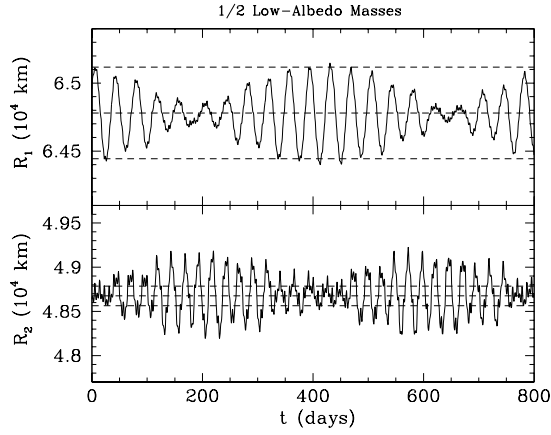


Fig. 6.— Same as Fig. 2, but for the numerical integration with P2 and P1 having half the low-albedo masses. The periodic variations in  $e_2$  and  $e_1$  have amplitudes that are significantly larger than in the high-albedo case (Fig. 3) and are visible without transforming  $R_2$  and  $R_1$  to  $R'_2$  and  $R'_1$ .

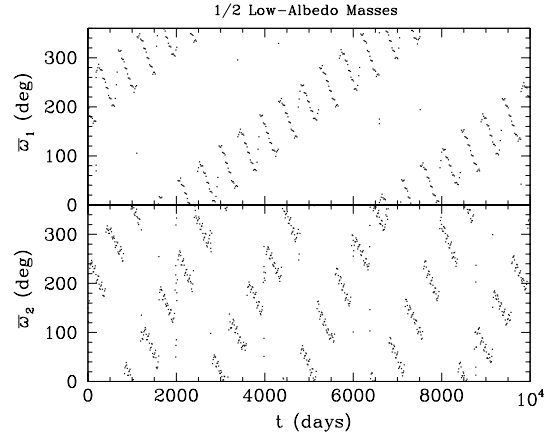


Fig. 7.— Same as Fig. 4, but for the numerical integration with P2 and P1 having half the low-albedo masses. Compared to the high albedo case (Fig. 4), the amplitudes of the short-term periodic variations are significantly larger, and the periods of the long-term prograde precession are slightly shorter.

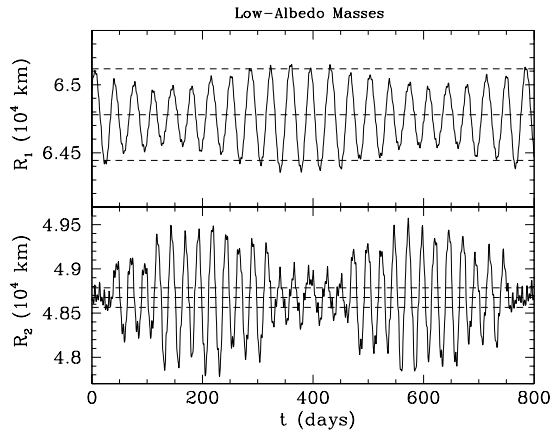


Fig. 8.— Same as Fig. 2, but for the numerical integration with the low-albedo masses for P2 and P1. The amplitude of the periodic variation in  $e_2$  continues to increase with mass, but that in  $e_1$  is smaller than in the case with half the low-albedo masses (Fig. 6).

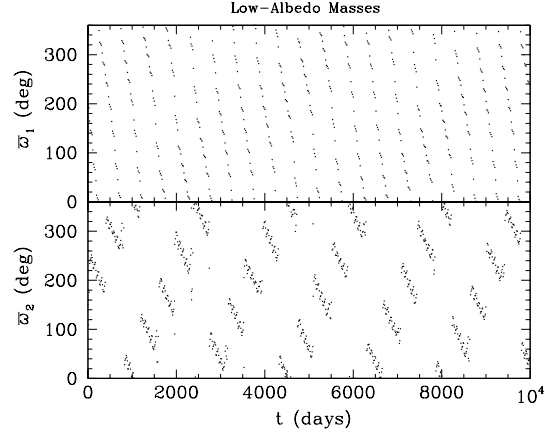


Fig. 9.— Same as Fig. 4, but for the numerical integration with the low-albedo masses for P2 and P1. While  $\varpi_2$  continues to show long-term prograde precession with large short-term periodic variation,  $\varpi_1$  shows a completely retrograde precession with a period of 500 days.

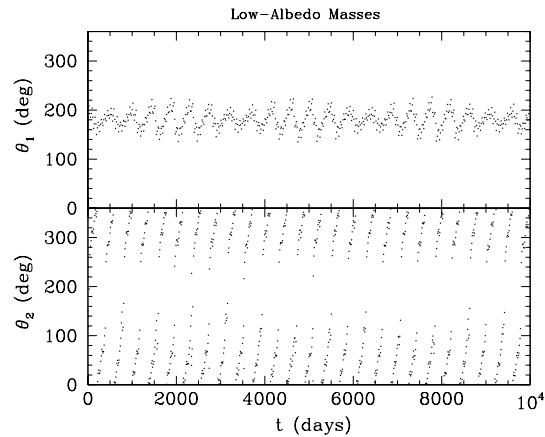


Fig. 10.— Same as Fig. 5, but for the numerical integration with the low-albedo masses for P2 and P1. While  $\theta_2$  circulates as in the high albedo case shown in Fig. 5 (the nearly empty region about  $180^\circ$  is due to the fast prograde precession of  $\varpi_2$  when  $e_2$  is small),  $\theta_1$  librates about  $180^\circ$ .



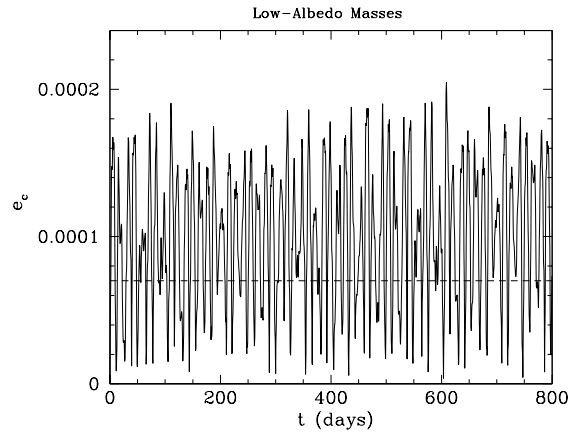


Fig. 11.— Variation in the orbital eccentricity  $e_c$  of Charon for 800 days in the numerical integration with the low-albedo masses for P2 and P1. The dashed line indicates  $e_c = 7.0 \times 10^{-5}$ , which is  $1 \sigma$  above the best-fit value ( $e_c = 0.0$ ) in Table 1.